Low Power Thermal Tuning in Resonant Vertical Junction Silicon Modulators Through Substrate Removal
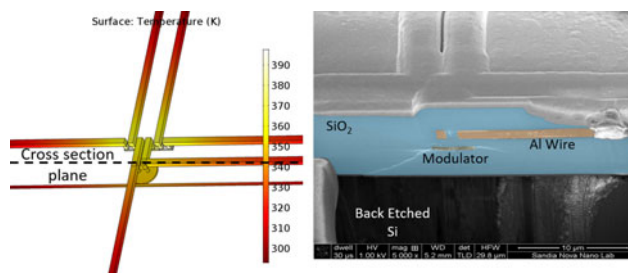
Nicholas Jacob D. Martinez
Christopher T. Derose
Robert Jarecki
A. L. Starbuck
Andrew T. Pomerene
Douglas C. Trotter
Anthony L. Lentine

IEEE

Low Power Thermal Tuning in Resonant Vertical Junction Silicon Modulators Through Substrate Removal

Nicholas Jacob D. Martinez , **Christopher T. Derose,**
Robert Jarecki, A. L. Starbuck, Andrew T. Pomerene,
Douglas C. Trotter, and Anthony L. Lentine

Sandia National Laboratories, Albuquerque, NM 87185 USA

Abstract: We report on thermally tunable modulators, with efficiencies up to 2.16 nm/mW. Efficient performance was accomplished through integrated heater design and Si substrate removal, where the heavily N+ doped Si heater element is integrated into the body of the microdisk. For comparison, modulators with an external heater design were also tested with small diameter Si substrate removed. The external heavily doped N+Si heater bars were fabricated outside the diameter of the microdisk. Efficiency for external heater design was 0.68 nm/mW with substrate removed. Both types of thermal modulators were experimentally tested and simulated for a complete understanding of the Si substrate's influence on heat dissipation with both types benefiting significantly from substrate removal. Agreement between simulation and experimental results was greater than 80% in all instances.

Index Terms: Optoelectronic materials, fabrication and characterization.

1. Introduction

Thermo-optically shifted silicon photonics microdisk resonator based filters and modulators offer a wide range of wavelength tunability. The thermal tunability is accomplished via the thermo-optic effect (TOE), whereby variation in the refractive index of the modulator is thermally induced [1], [2]. This is an ideal method for stabilizing devices, such as resonant modulators, which are typically fabricated across a large wafer and may have non-uniformity in their resonant frequency. One possible direct application of these devices is wavelength division multiplexing (WDM), where potentially thousands of modulators and filters are fabricated on a single chip with multiple optical input output (IO) connections. Undoubtedly, some will not be resonant at the intended wavelength(s) due to fabrication tolerances, and environmental temperature variations may cause the resonance to shift from their nominal room temperature values. Thermal tunability allows the modulators and filters to be stabilized at the intended resonance, despite modulator manufacturing and environmental variability. It can also be used to tune the resonance to a range of wavelengths versus a single intended one.

Because silicon has a weak dependence on primary electric field effects, like the Pockels, Kerr, and Franz-Keldysh effects [3], most silicon modulators make use of the plasma dispersion effect. As an example, small resonant carrier depletion type modulators often require a driving voltage less than 1 V and with their small size, can have a dynamic energy consumption of a less than a few femtojoules per bit [4]–[6]. While directly varying the carrier concentration can provide a small amount of tuning to compensate for temperature and manufacturing induced changes in resonant wavelength [7], thermal tuning allows a much greater tuning range. Unfortunately, devices that require significant thermal tuning may require a relatively large amount of power to get a usable translation in resonance, or correct a resonance that has been significantly changed from its desired wavelength because of the environment or fabrication variations. Therefore, it is very important that the thermal tuning be as efficient as possible to keep the overall energy consumption of the modulator as low as possible.

Significant effort has been put towards reducing the power consumption for dynamic optical switching in silicon modulators. Commensurate effort has also been done to improve the efficiency of thermal tuning in silicon modulators. The efficacy of thermal tuning by means of applied heater power is compounded by Silicons large thermo-optic coefficient. Materials include chromium [8] or other metal resistive types [9]–[11], doped silicon [4]–[6], [12], [13], and even graphene [14] on or in Si modulators used for thermal tunability. In 2014, Wade *et al.* fabricated an integrated heater, which currently stands at as the most efficient thermal modulator design [15], reaching an efficiency of 2.73 nm/mW. This efficiency was measured at 1300 nm and, unfortunately, requires complete substrate removal to achieve this efficiency.

Earlier in 2010, Dong *et al.* fabricated a free-standing racetrack thermally tunable resonator with an estimated 4.8 nm/mW [11], which is to our knowledge, the highest efficiency integrated thermally tunable resonant filter in silicon photonics. The high efficiency of their integrated heater design was demonstrated by creating an air trench below the racetrack resonator, in the substrate, and in the oxide, leaving a free-standing device. Also in 2010, Cunningham *et al.* [13] included the removal of the Si substrate as part of their process flow for their filters. Removing the substrate improved their efficiency by 20× although the result was not as efficient as the devices in [5] and [11]. That same year Masood *et al.* [16] included insulative air trenches with their removed substrate, with a similar 20× improvement in efficiency. Where both Cunningham *et al.* and Masood *et al.* see tremendous improvement possibly due to their devices being initially inefficient with substrate remaining. We also postulate that the improvement in performance is easier in a filter compared to a modulator, because the high-frequency conductive leads and doped regions of the modulator cause a compromise to be reached in the heater efficiency. We will discuss this more in the paper.

In this paper, we examine the effects that substrate removal has on our external heater modulators [17], as well as our high efficiency integrated heater modulator [5], which to date has the highest thermal tuning efficiency for resonant modulators without substrate removal. These are designed and fabricated in the same process as [10]. Both types of heater element designs are depicted in Fig. 1(a) and (b), and are implemented as n+ type resistive elements in silicon. Placing the heater outside of the domain of the microdisk is what is signified as an external heater. The heater elements placed within the interior of the modulator term the device an integrated heater modulator. We examine both types of heater modulators with their substrate removed in the vicinity of the devices and compare to the same devices with substrate remaining to improve the thermal tuning efficiency for a full spectrum of applications that may prioritize tuning efficiency over modulation speed, or vice versa. Wavelength scans were initialized around 1550 nm for the purposes of this testing.

The integrated heater design, shown in GDS format in Fig. 1(b), was one such design that embedded the heater within the microdisk modulator. Integrating the heater element is really the optimal way for efficiently thermally tuning the modulator because the thermal source has a low thermal impedance path to the optical mode. Another benefit to the integrated heater design is it enables a more compact device, leaving valuable fabrication real estate for other opto-electronic components. However, internally heating the modulator can reduce the performance of the device. Since current is flowing through the heater, some current may also flow through parts of the
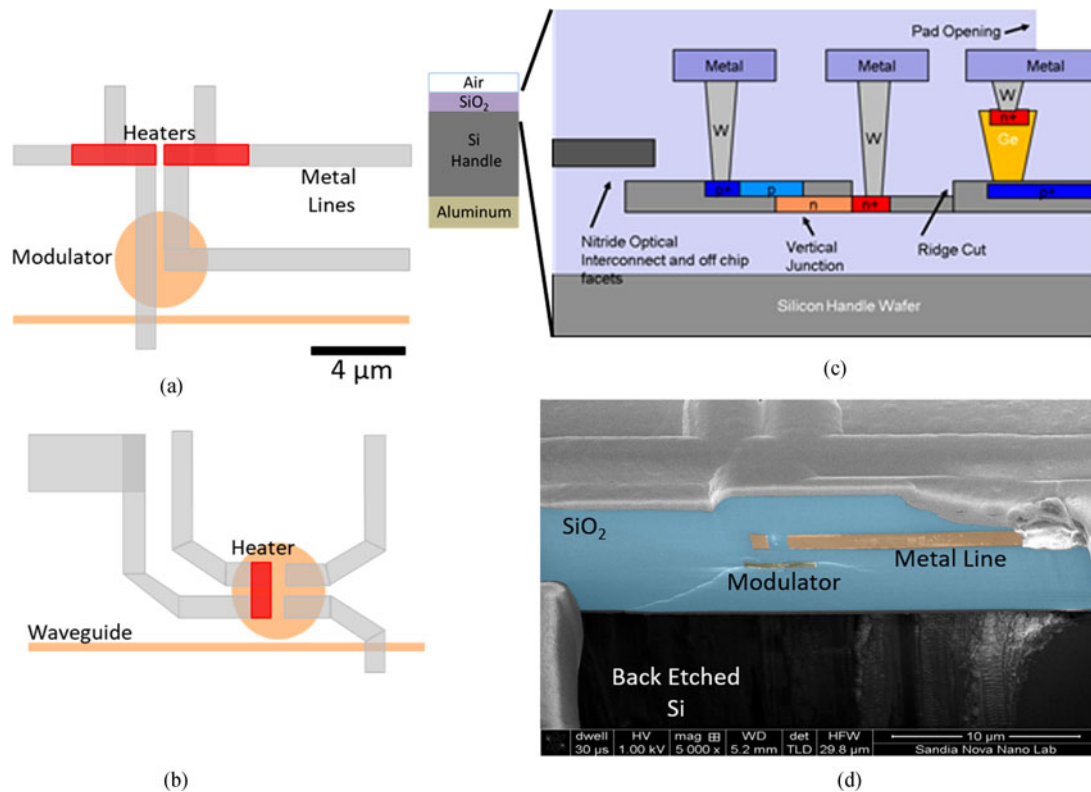
Fig. 1. Design and cross-sectional SEM of heater modulators. (a) Model of external heater design. (b) MOdel of integrated heater design. (c) Schematic representation of semiconductor and metallic layered components, not to scale. (d) SEM of external heater design with substrate removed. Note Si substrate has been removed up to oxide cladding.

modulator, inducing undesired carrier effect index change, and causing a resonance shift counter to that of the heater. Also, current from the integrated heater element can overlap with the mode profile of the signal, causing added absorption.

Lastly, that heater current in the modulator can limit the modulation bandwidth due to free carrier lifetime [18]. These deleterious effects of an integrated heater modulator are the premise for improving externally heated modulators with the heater outside the microdisk. Previously, bit error rate (BER) was measured at 10 Gb/s for both the integrated and external heater modulators [17]. Using the integrated heater modulator, DeRose *et al.* found a power penalty of 1 dB in receiver sensitivity at a BER of 1e-9 when the heater was enabled compared to that when it was disabled. However, the external heater showed no discernible power penalty when the heater was enabled. In addition, the receiver sensitivities when using the external heater modulator device was 3 dB better than the integrated heater modulator when the heaters were enabled, and 2 dB when disabled at the same measurement conditions. The power penalty referenced above provides evidence that the heater current in the integrated heater modulator degrades modulator performance, and the difference in receiver sensitivity between the two modulators shows that we can design a higher performance modulator when the heater is not integrated internal to the disk. The resonances show a Q of $\sim 10^4$ for our modulators near 4 μm diameter.

Our externally heated modulator, as seen in Fig. 1(a), has two symmetrically displaced heater elements 2 μm away from the edge of the microdisk modulator. The heater elements have improved thermal connection to the modulator through the Aluminum (Al) wires that connect to the modulator with Tungsten (W) vias. The connection acts purely as a thermal conduit and does not bias the p-n junction in the modulator. The heater is also placed on the opposite side, relative to the bus

waveguide, to minimize heating of the bus waveguide. Currently, our 4 μm diameter modulators used in both heater designs offer 58.6 nm free spectral range (FSR). The p-n junction has been left out of the GDS images in Fig. 1(a) and (b), but can be found in their references [5], [17].

2. Fabrication

The modulators were designed as part of Sandia's Silicon photonics process, described in [19]. In addition to the normal process flow, dry reactive ion etching (DRIE) was used in order to remove the Si Substrate for a nominal back etch hole of 60 μm diameter. With individual chips diced out for back etch processing, chips were sub-mounted to a 6 in. wafer, which served as the carrier. Substrate removal was targeted by stages of etching followed by confocal microscope inspection. Bosch-style DRIE etch (Plasma-Therm Versaline DSE-III) time was approximately 200 min with a cathode temperature of 20° C. A repeatedly-cycled 3-step sequence of deposition/etch A/etch B was used, with the deposition step at 150/30 standard cubic meters per minute (sccm) C_4F_8/Ar, 25 mTorr, 2000 W inductively coupled plasma (ICP) power, and -10 V_{DC} RF substrate bias, followed by an etch A step at 250/30 sccm SF_6/Ar, 50 mTorr, 2000 W ICP, -700 V_{DC}, and an etch B step at 450/30 sccm SF_6/Ar, 60 mTorr, 2500 W ICP, -10 V_{DC}. Step times were 4.0 s, 2.1 s, then 2.0 s respectively. From Fig. 1(c), it is clear the etching was uniformly done all the way to the oxide cladding, with minimal scalloping seen in the back-etched Si. Other substrate-removed modulators were verified through SEM, as well, and showed complete etching all the way to the SiO_2 cladding. Patterning was done with AZ9260 photoresist.

3. Device Simulations

Finite element method (FEM) software, COMSOL, was used for simulating heat transfer for the two types of heater modulators, with and without substrate removed. All simulations started with a 50 μm thick aluminum base layer. This initial aluminum layer served to represent the Thorlabs stage mount onto which the device under test (DUT) was placed. The next built layer was the 675 μm Si handle followed by an 8.5 μm SiO_2 cladding. An additional 50 μm layer of air was added last to represent convective heat transfer above the DUT. An example of the stacking and imbedded metallic components are seen in Fig. 1(c).

Referring to the optical images in Fig. 2, there are differences in Aluminum wire layout between the integrated and external heater design. The aluminum probe pads connected to the wires are also placed in a different pattern. As such, the area of all stacked layers, specifically for the internal heater design, were enlarged to ensure all metallic components, the components where thermal dissipation is most prevalent, were well away from the simulated boundary. It was seen in initial simulations that having the boundary in close proximity to metal components, such as the Al pads, allowed heat to travel directly from the metal to the boundary. Our first simulations confirmed, when simulated data was analyzed, to be much less efficient than experimental data. Therefore, in the simulations presented here, the layers were made wider and longer in order to ensure all embedded components were far enough from the boundary to mimic a 'bulk' material setting.

The stacked layers from the aluminum base layer to the air top layer were set to have the same length and width, which made converging on a minimum layer length and width parameter easier. In these simulations, the side boundaries were set 50 μm and 100 μm in the x and y dimensions beyond the farthest extent of the aluminum probe pads connected to the device. Decreasing the side dimensions less than this caused heat to conduct directly to the side boundaries, reducing the efficiency, however increasing them caused very little change to the results. This confirmed our choice of smaller bulk volume, or domain size, to be sufficient and did not adversely affect the thermal dissipation in the simulation. This is best illustrated in Fig. 2(a) and (b) lower images. These are taken straight from the FEM software and show the entire modeling volume.

All outer most surfaces of the stacked layers were set to a room temperature boundary condition. Applying these heat sink boundaries replicated the fabricated design, where all materials continue further and act as a pseudo-reservoir for the heat to flow in to. Since we were able to reduce the
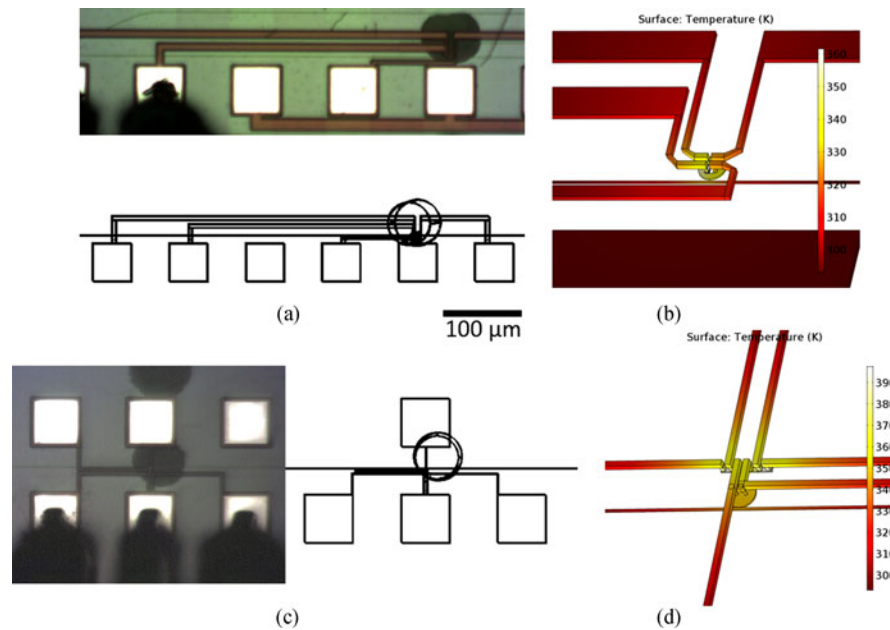
Fig. 2. Verifying simulation mimics experimental design. (a) Actual (above) and simulated (below) design of integrated heater modulator. (b) Thermal distribution of integrated heater modulator. (c) Actual (left) and simulated (right) design of external heater modulator. (d) Thermal distribution of external heater modulator.

overall simulated size of the geometry, a smaller mesh size, or tetrahedral meshing elements, was used to fill the volume of the material in the simulation. Mesh size was set to COMSOL's 'extremely fine' setting, with a minimum element size of 130 nm. This size was adequate given the waveguide and aluminum conduits, where heat was most readily conducted, are greater than 200 nm in their smallest dimension.

The Si, SiO_2, Al, tungsten (W), and air materials were all incorporated using COMSOL's materials list from the built-in library. The modulator and metallic components were embedded after all the stacked layers were built. For the modulator and metallic components built into the stacked layers, forming COMSOL's 'unions' were not required. COMSOL is designed to allow the creation of new domains, or volumes of interest, to replace the partial volume of the larger domain it occupies. This means the smaller W vias and Al wires can be built into the existing oxide layer, see Fig. 1(c), without conflict with the pre-existing SiO_2. Dimensions for the imbedded components were taken from the GDS file used for lithographical mask fabrication.

Specifically, for the heat transfer simulation for the integrated heater modulator, the Al wires were relatively wide with a linear Al pad layout. Therefore, the simulated bulk layers were designed with an overall width of 650 μm to avoid heat flow directly to the boundaries. As can be seen in the simulated design in Fig. 2(a) and (b), all pads near the microdisk were included. The simulated back-etched Si hole, nominally set to 60 μm, was relocated off center to replicate what was the final result of the experimental etch. The simulated hole was shifted away from the lower Al pad.

In the case of the heat transfer simulation for the external heater modulator, the Al wires were thinner in design with Al pads in a closer proximity to the modulator, shown in Fig. 2(c) and (d). Because of the more compact design, the simulated bulk layers were designed with an overall width of 400 μm. All three pads connected to the heater elements were simulated as well as the top Al pad designed for RF modulation control. The outer pads were not included since the right pad, seen in the real space image of Fig. 2(c), is electrically isolated and the left pad, which is also used for RF modulation, is far away. Initial simulations of previous external modulators with substrate remaining gave the same results with and without these two Al pads so they were removed to allow the simulation a finer mesh with a faster convergence rate.
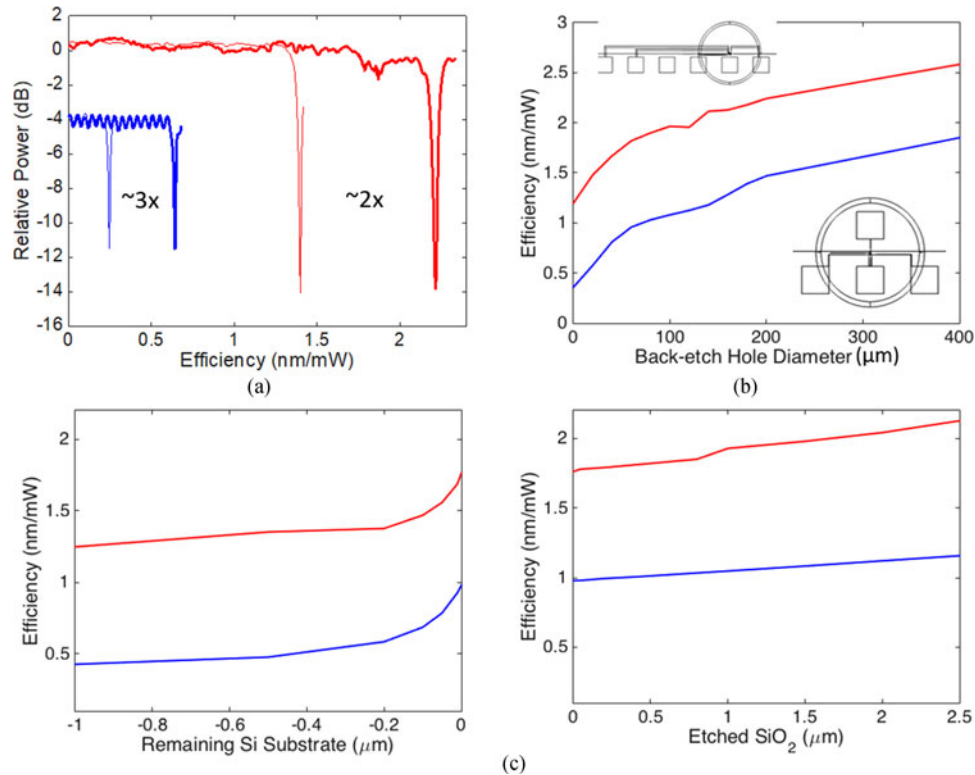
Fig. 3. Improved efficiency with Si substrate removed. (a) Experimental wavelength shift before and after substrate removal for external heater (blue) and integrated heater (red) design. The bold lines are with the substrate removed and the thin lines are without removal. (b) Simulated efficiency improvement for varying back etched diameter of Si substrate of external heater modulator. Simulated designs for 200 m diameter back etch shown. (c) Simulated wavelength shift dependence for Si remaining near Si/SiO$_2$ interface to the left. Simulated wavelength shift dependence for SiO$_2$ etched past SI/SiO$_2$ interface to the right. In both cases, power was kept constant.

Calculating the heat transfer was done first by interpreting the temperature change of the microdisk modulator when power was applied to the heater elements. The single integrated heater element and two symmetrical external heater elements were set as heat source domains in COMSOL. An overall heater-power was input into the simulation, 4.84 mW for the external heater and 2.32 mW for the integrated heater simulation. The difference in dissipated power is due to the external heater elements being larger and there being two heaters in comparison to the single integrated heater for the internal design. After convergence of the simulations, the temperature of over 100,000 points within the modulator was extracted for further analysis.

The FEM simulations were used to calculate the shift in relative permittivity, $\delta\epsilon_r$. First, room temperature (T_{RT}), or 293 K, is subtracted from the 3D FEM temperature matrix in order to calculate the change in temperature, dT as a function of spatial position (x, y, z). Next, the thermo-optic coefficients, dn/dT, for Si and SiO$_2$ are multiplied by the change in temperature, ΔT, to calculate the spatial change in refractive index. The thermo-optic coefficients used for Si [20] and SiO$_2$ [21] were

$$\frac{dn_{Si}}{dT} = 9.48 \cdot 10^{-5} + 3.47 \cdot 10^{-7} T - 1.49 \cdot 10^{-10} T^2 \tag{1}$$

and

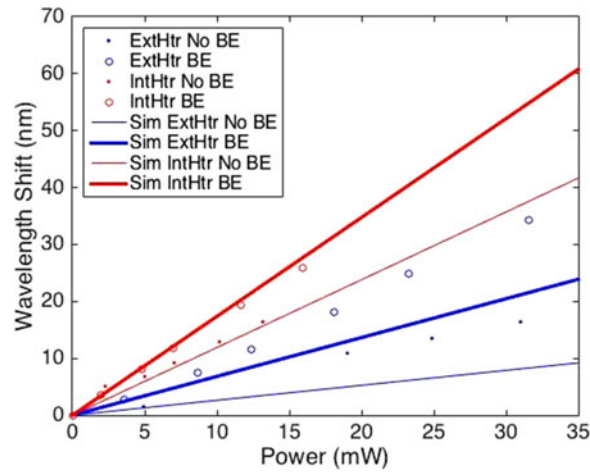$$\frac{dn_{SiO_2}}{dT} = 8.5 \cdot 10^{-6} / K \tag{2}$$

Fig. 4. Comparison of experimental and simulated results. Experimental data shown as open circles and dots. Simulated results are shown as lines. Blue (red) lines are for external (integrated) heater-modulators. No back-etch is denoted as No BE and devices with back-etch are denoted as BE.

respectively. From here it was simple conversion using the relationship between the square of the index of refraction and the permittivity. The change in permittivity, $d\epsilon_r$ is calculated from $2n\delta n$, where n is the refractive index and δn is the change in refractive index. Finite difference frequency domain (FDFD) software was used to calculate the electric field of the fundamental mode supported within the microdisk, which included an oxide cladding surrounding the microdisk for correct interpretation of the evanescent field. The electric field, E(x, y, z), was extracted from the FDFD software on a uniform grid. The output of the FEM simulation interpolated onto the same uniform grid. Finally, the change in resonant frequency per unit power dissipated is determined by calculating the overlap integral given by [22, eq. (3)]. Simulations showed our 4 μm microdisk to have a resonance at 1539 nm. This was the wavelength used for the conversion from frequency, v_0, to wavelength to calculate the efficiency in nm/mW.

$$\frac{dv}{dP} = \frac{v_0}{2} \frac{\int \int \int \frac{\delta \epsilon_r}{\delta P} |E|^2 dV}{\int \int \int \epsilon_r |E|^2 dV} \tag{3}$$

4. Characterization

Both heater modulator types were characterized using a tunable laser source (Agilent HP816x) at 0 and 0.5 V applied bias in to the heater circuit. The laser was fiber coupled to a polarization controller, which was then fiber coupled to the device. After identifying the decrease in throughput optical power associated with a resonance, the tunable laser was set to the wavelength at the resonance minimum. The polarization controller was then adjusted to ensure maximum resonance extinction. Wavelength sweeps were done from 1500 nm to 1600 nm in 0.01 nm increments with and without applied bias to the heater elements.

Voltage was supplied by a source-meter supply connected to GSG RF probes. Optical output power was recorded as a function of wavelength with and without applied bias to the heater elements. When a bias of 0.5 V was applied, the current was recorded in order to calculate the dissipated power. To keep consistency across tested modulators, 0.5 V was the standard used to measure the thermal efficiency. The same setup was used for both types of heater modulators, with and without the substrate removed. Heater resistance can be calculated given the known applied voltage and power from Fig. 4, however the heater elements were designed to have a resistance of 100 Ohms/square.

5. Theoretical and Experimental Data

Experimental results shown in Fig. 3(a) show a clear increase in wavelength shift for the same applied heater bias with the substrate removed compared to the devices with the substrate remaining. The blue (red) line is for the external (internal) heater modulator with the thicker line denoting wavelength shift after substrate removal. One thing to note is, although 0.5 V applied bias was used to measure all devices for thermal efficiency, the power dissipated by the external heater was nearly 2× that of the integrated heater element. This is made clear by referring back to Figs. 1 and 2. In Fig. 1(a) and (b), it is clear the external heater is composed of two elements with a relatively larger volume than the integrated heater. In Fig. 2(b) and (d), it is clear the external heaters are dissipating more heat compared to the integrated heater as seen by the temperature legend.

The devices with the substrate remaining had an efficiency of 0.26 nm/mW and 1.39 nm/mW for the external and internal heater modulators, respectively. These numbers are simply calculated by dividing the measured wavelength shift in nm by the applied power supplied to the heater as measured using the source meter. The devices with the substrate removed had an increased efficiency of 0.68 nm/mW and 2.16 nm/mW for the external and internal heater modulators, respectively.

Comparing the thermal simulations to experimental results showed an overall trend in the simulations having less wavelength shift for a given power dissipation in the heater element, i.e., less efficient. We believe that the added losses are due to setting the boundary conditions to room temperature with no thermal impedance. Since all the side boundaries are held at room temperature, they are effectively an infinite heat sink pulling heat away from the modulator more readily compared to experimental tests. However, the other choices would have been to use an infinite thermal impedance or one that was arbitrarily assumed to match the data, neither of which is likely to have given a more predictable measure of the results in advance of doing the measurements. However, agreement was still greater than 80% for the integrated heater design and greater than 93% for the external heater design, which is close enough to apply our simulations to device concepts or configurations that we didn't fabricate and couldn't measure.

Fig. 3(b) is a simulated wavelength shift for the integrated (external) heater modulator, shown in red (blue) as a function of back etch hole diameter up to a diameter of 200 μm. The overall Si handle is approximately 675 μm so it's important to know what effect hole diameter has on heat dissipation, specifically when efficiency has plateaued with increased hole diameter. There is slight variation at the 60 μm diameter from the other simulated results because here we assume the hole is perfectly aligned with the heater. Recall from Fig. 2 this was not the case. However, what is also important is that despite the back-etched hole simulated to only 200 μm, the efficiency is already approaching that of the Wade *et al.* [16] and does not require complete substrate removal.

Also, recall the simulations done in this work consistently suffered from lower efficiency that the actual measurements, so actual efficiency for a given back etch diameter would likely be higher. Nevertheless, increasing back etch hole diameter shows an increase in efficiency since the heat conducted through the metal lines must either travel through the oxide insulator cladding or remain in the metal. If the hole diameter were increased to be beyond the farthest metallic lines, the heat flow would be restricted by the oxide insulator cladding and poorly conductive air gap. The unfortunate prospect to this approach is the metallic probe pads would be completely unsupported and would likely be a mechanical failure point when electrically probed.

The left graph showing the simulated efficiency in Fig. 3(c) shows a dramatic increase in efficiency as the remaining substrate approaches zero. This feature is expected, as etching the Si reduces the thermally conductive path for heat dissipation. What can be surmised from the simulations on etching is that the Si is a much better conductor of heat and greatly effects the efficiency especially if not completely etched down to the oxide surface. The right simulated graph in Fig. 3(c) shows the efficiency change if etching continued into the oxide cladding. Efficiency does improve as etching continues towards the underside of the thermally tuned modulator, however, the improvement is minimal. Despite less than 1 nm of improved wavelength shift, oxide removal may be an additional step in processing to further enhance thermal efficiency.

TABLE 1
Efficiency Comparison

Efficiency [nm/mW]	Heater	Type	Substrate	Wavelength [nm]	Reference
0.13	External	Filter	Remaining	1550	Amatya et al. 2007 [8]
1.81	Internal	Filter	Remaining	1550	Watts et al. 2009 [10]
0.25	Hybrid	Filter	Removed	1540	Cunningham et al. 2010 [13]
4.8	External	Filter	Removed	1550	Dong et al. 2010 [11]
0.26	External	Resonator	Remaining	1575	Qiu et al. 2011 [7]
1.14	Internal	Modulator	Remaining	1550	Zortman et al. 2012 [5]
1.78	Internal	Filter	Remaining	1530	Timurdogan et al. 2012 [12]
1.02	Internal	Modulator	Removed	1550	Zheng et al. 2012 [23]
1.71	Internal	Modulator	Remaining	1580	Timurdogan et al. 2013 [24]
0.38	External	Modulator	Remaining	1550	DeRose et al. 2014 [17]
1.14	Internal	Modulator	Remaining	1580	Timurdogan et al. 2014 [6]
2.73	Internal	Modulator	Removed	1300	Wade et al. 2014 [15]
0.32	External	Modulator	Remaining	1550	Zheng et al. 2014 [9]
1.08	Internal	Resonator	Remaining	1530	Su et al. 2015 [25]
1.23	Internal	Resonator	Remaining	1180	Sun et al. 2016 [26]
0.48	Graphene	Resonator	Remaining	1540	Yu et al. 2016 [14]
2.16	Internal	Modulator	Removed	1550	This Work
0.68	External	Modulator	Removed	1550	This Work

Comparisons of this work to previous work was done and tabulated in Table 1. Important factors from each design are given, including efficiency, heater design, type of microdisk or microring used, whether or not the substrate was removed and what wavelength it was tested at. The table is organized according to publication date; however, internal heater devices with efficient designs have been shown in many instances. Substrate removal is beneficial for reducing unintended power dissipation, but clearly has not been adopted as part of a process flow for most of the published work above. For the devices with substrate removal, efficiency has improved up to 20× [13].

Additional simulations were done to mimic Dong's [11] fabricated devices where the oxide was etched away leaving a free-standing racetrack resonator. For our modulators, the center of the microdisk was not simulated, nor fabricated to have an air trench. In these subsequent simulations, oxide was only removed around the outside of the microdisk and in between the metal lines and waveguide because of the small diameter of our microdisk. The depth of the simulated air trench was comparable to the diameter of the modulator, about 4 μm. Simulations show the eternal heater modulator's efficiency increases by ∼2× to 1.25 nm/mW. Similarly, the efficiency of the integrated heater modulator increases by <1.5× to 2.46 nm/mW. The simulations show the metal lines as the consistent path for heat dissipation in all cases, becoming the major path when oxide is removed leaving a free-standing microdisk with waveguide and metal lines.

Our current designs with substrate removed do not benefit from such a large improvement in efficiency of up to 20× as others have observed. We believe our initial designs showed good efficiency [5], [17] prior to substrate removal, so efficiency gains after substrate removal did not have the expected benefit because the typical paths for heat loss had already been mitigated. For example, our external heater design entails coupling the heater element to the modulator through metal conduits. The metal lines improve efficiency by providing a much less resistive path for heat to flow to the modulator where as other external heater designs [7], [9] were built with the heater around the periphery of the disk or ring. The latter design implies heat will equally radiate towards and away from the ring or disk, dissipating energy into the bulk of the material.

Table 1 shows heater modulator/filter designs for the past 10 years, noting their efficiency, heater location, heater type, substrate status, and wavelength of operation. It's evident more work has been done for the benefit of internal heater designs, specifically because they start out more efficient in comparison to external heater designs. However, not nearly as much effort has been done to

mitigate the transfer of heat to the substrate, hence only four publications prior to this work where the substrate, to some extent, was removed below the modulator/filter. In the table, all of the most efficient heater-modulator designs are done with doped Si as heaters. This further corroborates what was seen in the simulations of metal conducting heat away from the modulator, thus reducing the efficiency.

Our efficiency comparison in Table 1 uses nm/mW as the metric, as more authors reference their efficiency this way versus other metrics. Some authors also quote efficiency relating to a free spectral range (FSR) or mW/FSR or FSR/mW [11]. In an ideal world, a heater of a fixed length, y, with an input power, P, changing the refractive index by a constant amount, dn, will have an efficiency in mW/FSR independent of the size of the device. However, the absolute wavelength shift in nm and the efficiency in nm/mW will be proportional to the diameter, radius, or circumference of the device. That is, a device with a 2 μm radius ideally has an efficiency in nm/mW that is double that of an identical device with a 4 μm radius, but the two devices have equal mW/FSR efficiencies.

Systems considerations are important for determining which metric is preferable. If we assume that we have to always tune an FSR in operation, then the metric relating to FSR is the most important. However, if we assume that we only need to tune a fixed wavelength range in nm or fixed temperature range in degrees that are less than an FSR, then the nm/mW is the more important metric. We could easily argue that as fabrication and material variations are reduced (or post-tuned) and the thermal tuning principally compensates for temperature variations, then the nm/mW is the more important metric. An example is a dense wavelength division multiplexed (DWDM) transmitter with 32 modulators with 200 GHz channel spacing with each modulator having a 6.4 THz FSR. The post-tuned fabrication tolerances might be ~100 GHz. We can argue then that the total tuning range required is the sum of the channel spacing plus the initial misalignment or 300 GHz, not the 6.4 THz FSR.

It's also harder to make smaller devices, particularly those with dopant contacts to a ring or disk because of the finite minimum size of the contacts and metal lines, and greater fabrication tolerances as a percent of dimensions (but not true in waveguide width of course). It is harder to make an efficient tunable modulator than a filter, and even harder to make an efficient small tunable modulator. This is because the high frequency leads and metals over modulator contacts take up a significant amount of space that can't be used for heating or isolating. The high frequency leads are a significant heat flow path that can't be eliminated; in a filter there are no such leads. While in theory a second level metal could be used for heating, similar to the filter in Dong *et al.* [11], the capacitance between that metal and the high frequency lines might also be of concern. As we showed, when simulating their approach, it did improve the efficiency (1.5×–2×) over the devices that we fabricated, but we could not remove enough oxide in simulation in the perimeter of the device to get to the 10×–20× improvement that some authors achieved in isolating their tunable filter devices.

Substrate removal requires accurate alignment, even for our modulators with a 4 μm diameter microdisk, so that the thermally conductive Si is removed from under the modulator and heater element. Having overlap of the heater circuit with unremoved substrate, such as our external heater modulators seen in Fig. 2(c), reduces the efficiency. But clearly even partially removing the substrate has its advantages as can be seen from Fig. 3(c). If cheaper and faster means of alignment and etching can be done, heater modulator designs with substrate removal could become standard practice, bringing thermal tuning capability to ultralow power efficiency. As we move forward, simulations will be key to verifying modulator and filter design to reach higher speeds with lower power requirements.

6. Conclusion

In this paper, we have described the design, fabrication, simulation, and characterization of an integrated heater modulator and an external heater modulator, with and without Si substrate removed. To our knowledge, it is the first paper that address local substrate removal of small (<4 μm dia.), thermally tunable vertical junction modulators, and the first to provide simulation results

corroborating experiment and showing the expected performance for an expanded design space including the size variations in etch hole diameter, etch depth, and the effect of added oxide isolation sections. Substrate removal has been verified to be fully through the Si handle, down to the oxide cladding. Ultimately, the previous efficient integrated heater design with substrate remaining saw nearly a $2\times$ improvement from 1.39 nm/mW, yielding an efficiency of 2.16 nm/mW. Similarly, the externally heated design with substrate removed elicited nearly a $3\times$ improvement at 0.68 nm/mW up from 0.26 nm/mW. In both designs, a factor of $1.5\times$–$2\times$ improvement over what we fabricated was found in simulation by removing the oxide selectively in some locations around the perimeter of the microdisk. With respect to the external heater design, future designs will incorporate adjustments to the heater shape to improve conduction to the microdisk, thus improving the efficiency.

Simulations have corroborated the experimental findings to an accuracy of $>80\%$. They have been paramount in identifying paths for thermal conduction away from the microdisk, which have already led to design improvements currently being fabricated for the external heater design. The metallic components clearly create a significant path for heat flow away from the modulator. Simulations of the heater modulators with substrate removed show heat traveling through the metal lines, when a back etch hole is present, before coupling into the Si handle. This explains why the most efficient heater modulator design is one with the substrate completely removed and the most efficient filter is fabricated with air insulation encompassing the microring.

For designs where the mechanical benefit the substrate offers cannot be sacrificed, simulations have shown efficiency as a function of back etch hole diameter. Efficiency increases with increasing back etch hole diameter because heat can either travel through the insulator oxide layer, or be retained around the metallic components as well as the modulator. Thus, if one is unwilling to compromise on structural integrity such as for a complete substrate removal process, this work has outlined the efficiency gain by adopting a simple back etch design, and expected efficiency gains for varying back etch diameters. And, with a proven simulation foundation, improvements can be verified, specifically for the external heater elements, potentially yielding a design that approaches the efficiency of the integrated heater design.

Acknowledgment

References

[1] N. Takato, K. Jinguji, M. Yasu, H. Toba, and M. Kawachi, "Silica-based single-mode waveguides on silicon and their application to guided-wave optical interferometers," *J. Lightw. Technol.*, vol. 6, no. 6, pp. 1003–1010, Jun. 1988.

[2] G. Treyz, "Silicon mach-zehnder waveguide interferometers operating at 1.3 μm," *Electron. Lett.*, vol. 27, no. 2, pp. 118–120, 1991.

[3] Z. Fang and C. Z. Zhao, "Recent progress in silicon photonics: a review," *ISRN Opt.*, vol. 2012, 2012, Art. no. 428690.

[4] W. A. Zortman, A. L. Lentine, D. C. Trotter, and M. R. Watts, "Low-voltage differentially-signaled modulators," *Opt. Exp.*, vol. 19, no. 27, pp. 26017–26026, 2011.

[5] W. Zortman, A. Lentine, D. Trotter, and M. Watts, "Integrated cmos comaptible low power 10 gbps silicon photonic heater modulator," in *Proc. Opt. Fiber Commun. Conf.*, 2012, Paper OW4I–5.

[6] E. Timurdogan, C. M. Sorace-Agaskar, J. Sun, E. S. Hosseini, A. Biberman, and M. R. Watts, "An ultralow power athermal silicon modulator," *Nature Commun.*, vol. 5, 2014, Art. no. 4008.

[7] C. Qiu, J. Shu, Z. Li, X. Zhang, and Q. Xu, "Wavelength tracking with thermally controlled silicon resonators," *Opt. Exp.*, vol. 19, no. 6, pp. 5143–5148, 2011.

[8] R. Amatya *et al.*, "Low power thermal tuning of second-order microring resonators," in *Proc. Conf. Lasers Electro-Opt.*, 2007, pp. 1–2.

[9] X. Zheng *et al.*, "A high-speed, tunable silicon photonic ring modulator integrated with ultra-efficient active wavelength control," *Opt. Exp.*, vol. 22, no. 10, pp. 12628–12633, 2014.

[10] M. R. Watts, W. A. Zortman, D. C. Trotter, G. N. Nielson, D. L. Luck, and R. W. Young, "Adiabatic resonant microrings (arms) with directly integrated thermal microphotonics," in *Proc. Conf. Lasers Electro-Opt./Conf. Quantum Electron. Laser Sci. Conf.*, 2009, pp. 1–2.

[11] P. Dong *et al.*, "Wavelength-tunable silicon microring modulator," *Opt. Exp.*, vol. 18, no. 11, pp. 10941–10946, 2010.

[12] E. Timurdogan *et al.*, "Automated wavelength recovery for microring resonators," in *Proc. Conf. Lasers Electro-Opt.*, 2012, pp. 1–2.

[13] J. E. Cunningham *et al.*, "Highly-efficient thermally-tuned resonant optical filters," *Opt. Exp.*, vol. 18, no. 18, pp. 19055–19063, 2010.

[14] L. Yu, Y. Yin, Y. Shi, D. Dai, and S. He, "Thermally tunable silicon photonic microdisk resonator with transparent graphene nanoheaters," *Optica*, vol. 3, no. 2, pp. 159–166, 2016.

[15] M. T. Wade *et al.*, "Energy-efficient active photonics in a zero-change, state-of-the-art cmos process," in *Proc. Opt. Fiber Commun. Conf. Exhib.*, 2014, Paper Tu2E–7.

[16] A. Masood *et al.*, "Comparison of heater architectures for thermal control of silicon photonic circuits," in *Proc. IEEE 10th Int. Conf. Group IV Photon.*, 2013, pp. 83–84.

[17] C. T. DeRose, R. Kekatpure, A. Starbuck, A. Pomerene, and A. L. Lentine, "A cmos compatible external heater-modulator," in *Proc. Opt. Interconnects Conf.,* 2014, pp. 17–18.

[18] D. K. Schroder, "Carrier lifetimes in silicon," *IEEE Trans. Electron Devices*, vol. 44, no. 1, pp. 160–170, Jan. 1997.

[19] M. R. Watts, W. A. Zortman, D. C. Trotter, R. W. Young, and A. L. Lentine, "Vertical junction silicon microdisk modulators and switches," *Opt. Exp.*, vol. 19, no. 22, pp. 21989–22003, 2011.

[20] D. B. Leviton and B. J. Frey, "Temperature-dependent absolute refractive index measurements of synthetic fused silica," *Proc. SPIE*, vol. 6273, 2006, Art. no. 62732K.

[21] G. Cocorullo, F. D. Corte, and I. Rendina, "Temperature dependence of the thermo-optic coefficient in crystalline silicon between room temperature and 550 k at the wavelength of 1523 nm," *Appl. Phys. Lett.*, vol. 74, no. 22, pp. 3338–3340, 1999.

[22] S. G. Johnson, M. Ibanescu, M. Skorobogatiy, O. Weisberg, J. Joannopoulos, and Y. Fink, "Perturbation theory for maxwells equations with shifting material boundaries," *Phys. Rev. E*, vol. 65, no. 6, 2002, Art. no. 066611.

[23] X. Zheng *et al.*, "Enhanced optical bistability from self-heating due to free carrier absorption in substrate removed silicon ring modulators," *Opt. Exp.*, vol. 20, no. 10, pp. 11478–11486, 2012.

[24] E. Timurdogan, C. M. Sorace-Agaskar, E. S. Hosseini, G. Leake, D. D. Coolbaugh, and M. R. Watts, "Vertical junction silicon microdisk modulator with integrated thermal tuner," in *Proc. Conf. Lasers Electro-Opt.*, 2013, pp. 1–2.

[25] Z. Su *et al.*, "An interior-ridge silicon microring switch with integrated thermal tuner," in *Proc. Integr. Photon. Res., Silicon Nanophoton.*, 2015, Paper IM2B–5.

[26] C. Sun *et al.*, "A 45 nm soi monolithic photonics chip-to-chip link with bit-statistics-based resonant microring thermal tuning," in *Proc. IEEE Symp. VLSI Circuits.*, 2015, pp. C122–C123.